NATIONAL ADVISORY COMMITTEE FOR AERONAUTICS

TECHNICAL NOTE 3587

IMPINGEMENT OF WATER DROPLETS ON A SPHERE

By Robert G. Dorsch, Paul G. Saper, and Charles F. Kadow

Lewis Flight Propulsion Laboratory
Cleveland, Ohio

Washington
November 1955

NATIONAL ADVISORY COMMITTEE FOR AERONAUTICS

TECHNICAL NOTE 3587

IMPINGEMENT OF WATER DROPLETS ON A SPHERE

By Robert G. Dorsch, Paul G. Saper, and Charles F. Kadow

SUMMARY

Droplet trajectories about a sphere in ideal fluid flow were calculated. From the calculated droplet trajectories the droplet impingement characteristics of the sphere were determined.

Impingement data and equations for determining the collection efficiency, the area, and the distribution of impingement are presented in terms of dimensionless parameters. The range of flight and atmospheric conditions covered in the calculations was extended considerably beyond the range covered by previously reported calculations for the sphere.

INTRODUCTION

One of the important factors in the design and evaluation of thermal icing-protection systems is the determination of the cloud-droplet impingement characteristics of the various components requiring protection. The placement of instruments that are sensitive to impinging atmospheric water droplets and ice accretions in the nose region of aircraft and missiles makes it increasingly important to provide protection for this area. An aircraft radar system, for example, is affected by a layer of ice or water distributed over the radome surface.

A portion of a prolate ellipsoid of revolution is frequently a good approximation to the nose region of an aircraft or missile. For this reason, theoretical droplet impingement calculations on prolate ellipsoids of revolution have been made by several investigators. Impingement calculations for ellipsoids varying in fineness ratio from 1 (a sphere) to 10 are reported in references 1 to 6.

In addition to their use in determining the impingement of cloud droplets on aircraft components, the impingement characteristics of the ellipsoid family are of interest in other fields such as chemical engineering and physical meteorology. For example, reference 7 shows

that the growth of a rain drop due to accretion as it falls through small cloud droplets can be calculated by using the collection efficiency of a sphere.

In contrast to the ellipsoids of other fineness ratios, the available differential-analyzer calculations of droplet impingement on the sphere (ref. 1) cover a very limited range of flight and atmospheric conditions. Therefore, it has been necessary to use theoretical and empirical extrapolation equations based on very limited calculated data in order to determine the impingement characteristics of the sphere at many of the physical conditions of interest.

The calculated droplet impingement data for the sphere presented herein are a continuation of the study of droplet impingement on prolate ellipsoids of revolution reported in references 3 and 4. The purpose of this report is to extend the range of published droplet impingement data for the sphere in ideal fluid flow. Droplet trajectories were computed at the NACA Lewis laboratory with the aid of an electromechanical differential analyzer. From the computed trajectories, the rate, distribution, and surface extent of impinging water were obtained and are summarized in terms of dimensionless parameters which cover a wide range of flight and atmospheric conditions.

SYMBOLS

The following symbols are used in this report:

C_D	drag coefficient for droplets, dimensionless
d	droplet diameter, microns
E_m	collection efficiency, dimensionless
K	inertia parameter, $1.704 \times 10^{-12}\ Ud^2/\mu R$, dimensionless
R	radius of sphere, ft
Re	local Reynolds number with respect to droplet, dimensionless
Re_0	free-stream Reynolds number with respect to droplet, $4.813 \times 10^{-6}\ d\rho_a U/\mu$, dimensionless
r,z	cylindrical coordinates, ratio to radius, dimensionless
r_0	starting ordinate at $z = -\infty$ of droplet trajectory, ratio to radius, dimensionless

$r_{0,tan}$ starting ordinate at $z = -\infty$ of droplet trajectory tangent to surface of sphere, ratio to radius, dimensionless

S distance along surface of sphere from forward stagnation point to point of droplet impingement, ratio to radius, dimensionless

S_m limit of impingement zone, ratio to radius, dimensionless

U free-stream velocity, or flight speed, mph

u local air velocity, ratio to free-stream velocity

v local droplet velocity, ratio to free-stream velocity

W rate of impingement of water, lb/hr

W_m total rate of impingement of water on surface of sphere, lb/hr

W_β local rate of impingement of water, lb/(hr)(sq ft)

w liquid-water content in cloud, g/cu m

β local impingement efficiency, $\frac{r_0}{r}\frac{dr_0}{dS}$, dimensionless

β_0 local impingement efficiency at stagnation point, dimensionless

μ viscosity of air, slugs/(ft)(sec)

ρ_a density of air, slugs/cu ft

τ time scale, dimensionless

Subscripts:

r radial component

z axial component

CALCULATION OF DROPLET TRAJECTORIES

As discussed in reference 3, the dimensionless equations of motion of droplet trajectories about a body in axisymmetric flow are of the same form as those derived in reference 8 for two-dimensional flow.

Using the same coordinate system (fig. 1) as that used for the prolate ellipsoid in reference 3, the dimensionless equations of motion for the z,r plane can be written

$$\left.\begin{aligned}\frac{dv_z}{d\tau} &= \frac{C_D Re}{24}\frac{1}{K}(u_z - v_z)\\ \frac{dv_r}{d\tau} &= \frac{C_D Re}{24}\frac{1}{K}(u_r - v_r)\end{aligned}\right\} \tag{1}$$

where

$$K = 1.704\times10^{-12}\frac{Ud^2}{\mu R} \tag{2}$$

The Reynolds number with respect to the droplet Re is obtained in terms of the free-stream Reynolds number

$$Re_0 = 4.813\times10^{-6}\frac{d\rho_a U}{\mu} \tag{3}$$

from the relation

$$\left(\frac{Re}{Re_0}\right)^2 = (u_z - v_z)^2 + (u_r - v_r)^2 \tag{4}$$

The equations of motion (1) of the droplet trajectories in the z,r plane are solved and summarized in terms of the dimensionless parameters Re_0 and K. From the droplet trajectories in the z,r plane, the droplet impingement characteristics of the sphere can be obtained.

The air-flow field around the body, required for the solution of the equations, was obtained from the classical equation for nonviscous, incompressible fluid flow about a sphere. The z- and r-components of the velocity can be expressed in the form

$$u_z = 1 - \frac{1}{2}\frac{(2z^2 - r^2)}{(z^2 + r^2)^{5/2}} \tag{5}$$

$$u_r = -\frac{3}{2}\frac{zr}{(z^2 + r^2)^{5/2}} \tag{6}$$

The values of the dimensionless air-velocity components u_z and u_r were calculated with the aid of digital computers for several hundred

points in the flow field. From the computed velocity values, input charts were constructed on glass cloth for the input tables of the differential analyzer used to calculate the trajectories. The values of the air velocity components u_z and u_r are given in figure 2. Figure 2(a) gives u_z as a function of z for constant values of r, while figure 2(b) gives u_r as a function of r for constant values of z.

The trajectories were calculated on the Lewis laboratory electromechanical differential analyzer; the characteristic features of the electromechanical differential analyzer are described in the appendix. The procedure for calculating trajectories of cloud droplets with respect to the sphere is basically the same as that described in references 3 and 8 for similar calculations on the mechanical differential analyzer or analog.

The equations of motion of the droplet trajectories were solved for various values of the parameter Re_0 between 0 and 8192. For each value of Re_0, a series of trajectories was computed for each of several values of $1/K$ between 0.0033 and 45. In order that these dimensionless parameters have more physical significance in the following discussions, some typical combinations of K and Re_0 are presented in table I in terms of the radius and the velocity of the sphere, the droplet size, and the flight pressure altitude and temperature.

Because the sphere is an aerodynamically blunt body, it disturbs the air-flow field for a considerable distance upstream. The solution of the droplet trajectories was performed, therefore, in three stages by separately solving the part of each trajectory within each of the three following regions: (1) $z = -15$ to -5, (2) $z = -5$ to -2, and (3) $z = -2$ to 0. When the solution of the trajectories was divided into three parts, the optimum scale factors for each of the three regions could be used; thus, the accuracy was considerably improved over that which would be obtained with a single solution from $z = -15$ to 0. Tests showed that starting at $z = -15$ was equivalent to starting the droplet at $z = -\infty$ as the change in droplet ordinate and velocity between $z = -\infty$ and $z = -15$ would have been negligibly small. The starting conditions at $z = -15$ were taken, therefore, to be those of the air stream at the chosen ordinate. The starting conditions at $z = -5$ and $z = -2$ were obtained from plots of the droplet velocities and ordinates (for the given Re_0 and K) at the end points of the previous interval.

RESULTS AND DISCUSSION

A series of droplet trajectories about the sphere was computed for the various combinations of the dimensionless parameters K and Re_0. The data obtained from these trajectories are summarized in figure 3, where the starting ordinate r_0 of each trajectory is given as a function of the point of impingement on the surface S (the distance measured along the surface from the forward stagnation point (-1.0, 0, fig. 1) to the point of impingement). Because S is made dimensionless by dividing by the radius of the sphere, it is also equal to the angle (in radians) between the z-axis and the radius vector to the point of impingement. The dashed lines in figure 3 are the loci of the termini of the constant K curves. These loci were found to be the same, within the order of accuracy of the computations, for all values of Re_0, as can be seen by comparing figures 3(a) to (g). Because droplets with infinitely large K would travel in straight lines in the free-stream direction, the $1/K = 0$ curve is obtained from the relation between r and S for a circle. From the data presented in this figure, the rate, area, and distribution of water-droplet impingement on the surface of the sphere can be determined for given values of Re_0 and K.

Total Rate of Impingement of Water

In flight through clouds composed of droplets of uniform size, the total amount of water in droplet form impinging on the sphere is determined by the amount of water contained in the volume within the surface formed by the tangent trajectories (fig. 1). Therefore, the total rate of impingement of water (lb/hr) can be determined from the relation

$$W_m = 0.33\pi w R^2 U r_{0,tan}^2 \tag{7}$$

where 0.33 is a conversion factor, the flight speed U is in miles per hour, liquid-water content w is in grams per cubic meter, and R is in feet. When constants are combined,

$$W_m = 1.04 w R^2 U r_{0,tan}^2 \tag{8}$$

In this equation, $r_{0,tan}^2$ is equal to the collection efficiency ($E_m = r_{0,tan}^2$) defined as the ratio of the actual amount of water intercepted by the sphere to the total amount of water in droplet form contained in the volume swept out by the sphere.

The value of $r_{0,tan}$ for a given combination of Re_0 and K can be obtained from figure 3 by determining the value of r_0 which corresponds to the maximum S for the constant K curve of interest. The values of $r_{0,tan}$ fall on the dashed termini curves of figure 3. In order to facilitate interpolation and extrapolation, the data are replotted in the form of $r^2_{0,tan}$ as a function of K for various constant values of Re_0 in figure 4. Examination of figure 4 shows that $r^2_{0,tan}$ increases with increasing K but decreases with increasing Re_0. At values of K less than 0.10, $r^2_{0,tan}$ approaches zero. It was not possible to determine from the differential-analyzer calculations whether or not a critical value of K exists (as suggested in ref. 1) below which there is no droplet impingement on the sphere. However, for K less than the critical value given in reference 1 (K = 0.083) the collection efficiency is certainly very small and is approaching zero.

The accuracy in the determination of $r_{0,tan}$ from the calculated trajectories is about of the same order for the sphere as for the ellipsoid of fineness ratio 5 (ref. 3). For values of $r_{0,tan}$ greater than 0.10, $r_{0,tan}$ was determined with an accuracy of the order of ± 0.005. For reported values of $r_{0,tan} < 0.10$, the accuracy of determining the tangent is more indefinite but appears to be within ± 0.01.

Extent of Droplet Impingement Zone

The extent of the droplet impingement zone on the surface of the sphere is obtained from the tangent trajectories (fig. 1). The point of tangency determines the rearward limit of the impingement zone. The limit of impingement S_m for a particular Re_0 and K condition can be determined from the maximum S value of the constant K curves of interest in figure 3. Again, to facilitate interpolation, the data are replotted in the form of S_m as a function of K for constant Re_0 values in figure 5. The data of this figure indicate that S_m increases with increasing K but decreases with increasing Re_0. A comparison of figures 4 and 5 shows that at values of K less than 0.1, S_m approaches zero much more slowly than the collection efficiency $r^2_{0,tan}$. The collection efficiency is practically zero in most of the region between K = 0.01 and 0.10, while S_m is still quite large. This difference can be explained by the fact that for small values of K only droplets starting close to the stagnation line (-z-axis) will

impinge on the sphere; however, the trajectories of these droplets are such that in the neighborhood of the sphere their path is almost parallel to the surface. Thus, they may travel a sizeable distance along the surface of the sphere before impinging even though the amount of water collected on the surface is very small.

Because of the difficulty of determining the exact point of tangency on the surface of the sphere of each tangent trajectory, the accuracy of determining S_m for each K and Re_0 condition is of the order of ± 0.020. Because the S_m data points were closely distributed about a common termini curve (fig. 3) for all values of Re_0 and K, the error in the values of S_m taken from the best-fit termini curve and replotted in figure 5 is of the order of ± 0.01. The accuracy in determining the values of S for the intermediate points of impingement given in figure 3 was much higher because the points at which the intermediate trajectories terminated on the surface of the sphere were much better defined.

Distribution of Impinging Water Along Surface of Sphere

The amount of water impinging on the surface of the sphere within any ring of width $S_2 - S_1$ can be determined if the starting ordinates r_0 are known for the droplets that impinge at S_1 and S_2. These data can be obtained from figure 3.

The amount of water (lb/hr) impinging within the ring of width $S_2 - S_1$ is given by the relation

$$W = 1.04(r_{0,2}^2 - r_{0,1}^2)wR^2U \tag{9}$$

Local Rate of Impingement of Water

The local rate of impingement of water in droplet form (lb/(hr)(sq ft)) on the surface of the sphere can be determined from the expression

$$W_\beta = 0.33Uw \frac{r_0}{r} \frac{dr_0}{dS} = 0.33Uw\beta \tag{10}$$

where β is the local impingement efficiency. The values of β as a function of S for combinations of Re_0 and K are presented in figure 6. These curves were obtained by multiplying the slope of the

curves in figure 3 by the corresponding ratio r_0/r at each point. Because the slopes of the r_0 against S curves (fig. 3) in the region between $S = 0$ and $S = 0.05$ are difficult to determine, the exact values of β between $S = 0$ and $S = 0.05$ are not known. The values of β presented in this region between $S = 0$ and $S = 0.05$ are estimated to be accurate within ± 0.05. A plot of the local impingement efficiency β_0 at the stagnation point ($S = 0$) as a function of K is shown in figure 7. The local impingement efficiency at $S = 0$ is sometimes useful as a parameter in empirical equations for calculating local impingement efficiency (ref. 2).

IMPINGEMENT IN CLOUDS OF NONUNIFORM DROPLET SIZE

The data presented in figures 3 to 7 apply directly only to flights in clouds composed of droplets that are all uniform in size. The droplets in a cloud, however, may have a range of sizes. Theoretical calculations and experience in the Lewis icing research tunnel on bodies of revolution have shown that the amount of ice collected when a distribution of droplet sizes is present in the tunnel is considerably different from that which would be obtained if only droplets of the volume-median size were present. Therefore, if the size distribution of the cloud-droplets is known or can be estimated, then the data must be accordingly modified (or weighted) before the rate, extent, and distribution of droplet impingement on the sphere are calculated. Methods of weighting the impingement data for a given droplet-size distribution are described in detail in reference 9.

CONCLUDING REMARKS

Because the droplet trajectories were calculated for incompressible, ideal fluid flow, a question may arise as to their applicability at the higher subsonic velocities. Reference 10 shows that the effect of compressibility on the impingement characteristics of a circular cylinder is small. Therefore, it is expected that the assumption of incompressibility does not invalidate the application of the calculated values at high subsonic velocities. A more serious deviation from ideal fluid flow is caused by the separation of the boundary layer from the surface of the sphere in the region between 70° and 90° from the stagnation point because of viscous effects. It is not known with certainty what effect the flow separation would have on droplet trajectories, but it is expected that except for large values of K (where the tangent trajectory touches within the separation region) the droplet impingement pattern would differ little from that calculated for the ideal fluid. At large values of K the effect is probably more pronounced, and

experimental tests would be required to establish the degree of agreement with ideal fluid calculations. In addition to any possible effects on the impingement pattern on the windward side of the sphere, the low-pressure eddy region on the leeward side of the sphere caused by flow separation may entrain some of the smaller droplets and cause some impingement on the lee side of the sphere.

Lewis Flight Propulsion Laboratory
National Advisory Committee for Aeronautics
Cleveland, Ohio, September 28, 1955

APPENDIX - DESCRIPTION OF LEWIS ELECTROMECHANICAL DIFFERENTIAL ANALYZER

The electromechanical differential analyzer is basically similar to the mechanical differential analyzer, or analog, described in appendix A of reference 8. The electromechanical differential analyzer has 10 integrators, 10 variable coefficients, 17 fixed coefficients, and 8 adders, all of which are synchro-coupled through an electric patch board. The electric interconnections between the various units used in problem programing are made at the patch board.

The variable coefficients are ball and disk integrators used as a multiplier by keeping the ball at one position throughout a solution. The ball is moved by hand cranking to the proper position on the disk before each solution is started. A counter, geared to the crank shaft, indicates the value of the coefficient. Five of these units can multiply by numbers from 0 to 2; the other five units can use factors up to 6. By switching, the factors can be made either plus or minus. Each of the variable coefficients has an electronic-servo amplifier to increase the available torque for rotating its disk.

The ten integrators each have two electronic-servo amplifiers, one for rotating the disk and one for moving the ball carriage across the disk. The lead screw of each integrator is geared to a counter that indicates the position of the ball on the disk.

Each fixed coefficient consists of a synchronous repeater and a synchronous transmitter connected by the proper gears.

The adders are synchro-differential motors, which assume a mechanical position proportional to the algebraic sum of two input signals. The motors are mechanically coupled to synchronous transmitters.

There are three input tables for supplying graphical data (such as air-velocity components) and one large output table that can simultaneously plot two functions against a single independent variable. Problem solutions are obtained from the output-table graphical plots or are read from mechanical counters coupled to the differential analyzer.

REFERENCES

1. Langmuir, Irving, and Blodgett, Katherine B.: A Mathematical Investigation of Water Droplet Trajectories. Tech. Rep. No. 5418, Air Materiel Command, AAF, Feb. 19, 1946. (Contract No. W-33-038-ac-9151 with General Electric Co.)

2. Torgeson, W. L., and Abramson, A. E.: A Study of Heat Requirements for Anti-Icing Radome Shapes with Dry and Wet Surfaces. WADC Tech. Rep. 53-284, Wright Air Dev. Center, Wright-Patterson Air Force Base, Sept. 1953. (Contract AF 33(616)-85, RDO No. 664-802.)

3. Dorsch, Robert G., Brun, Rinaldo J., and Gregg, John L.: Impingement of Water Droplets on an Ellipsoid with Fineness Ratio 5 in Axisymmetric Flow. NACA TN 3099, 1954.

4. Brun, Rinaldo J., and Dorsch, Robert G.: Impingement of Water Droplets on an Ellipsoid with Fineness Ratio 10 in Axisymmetric Flow. NACA TN 3147, 1954.

5. Dorsch, Robert G., and Brun, Rinaldo J.: Variation of Local Liquid-Water Concentration about an Ellipsoid of Fineness Ratio 5 Moving in a Droplet Field. NACA TN 3153, 1954.

6. Brun, Rinaldo J., and Dorsch, Robert G.: Variation of Local Liquid-Water Concentration about an Ellipsoid of Fineness Ratio 10 Moving in a Droplet Field. NACA TN 3410, 1955.

7. Langmuir, Irving: The Production of Rain by a Chain Reaction in Cumulus Clouds at Temperatures above Freezing. Jour. Meteorology, vol. 5, no. 5, Oct. 1948, pp. 175-192.

8. Brun, Rinaldo J., and Mergler, Harry W.: Impingement of Water Droplets on a Cylinder in an Incompressible Flow Field and Evaluation of Rotating Multicylinder Method for Measurement of Droplet-Size Distribution, Volume-Median Droplet Size, and Liquid-Water Content in Clouds. NACA TN 2904, 1953.

9. von Glahn, Uwe H., Gelder, Thomas F., and Smyers, William H., Jr.: A Dye-Tracer Technique for Experimentally Obtaining Impingement Characteristics of Arbitrary Bodies and a Method for Determining Droplet Size Distribution. NACA TN 3338, 1955.

10. Brun, Rinaldo J., Serafini, John S., and Gallagher, Helen M.: Impingement of Cloud Droplets on Aerodynamic Bodies as Affected by Compressibility of Air Flow Around the Body. NACA TN 2903, 1953.

TABLE I. - RELATION OF DIMENSIONLESS PARAMETERS TO BODY SIZE AND ATMOSPHERIC AND FLIGHT CONDITIONS

Atmospheric condition	Velocity of sphere, U, mph	Droplet diameter, d, microns	Radius, R, ft	Pressure altitude, ft								
				5000			15,000			25,000		
				Temperature, °F								
				20			1			-25		
				Re_0	K	1/K	Re_0	K	1/K	Re_0	K	1/K
Cloud droplets	50	10	0.3	14.7	0.08123	12.31	10.72	0.08383	11.93	7.836	0.08793	11.37
			3	14.7	.008123	123.1	10.72	.008383	119.3	7.836	.008793	113.7
			10	14.7	.002437	410.3	10.72	.002515	397.6	7.836	.002638	379.1
		50	0.3	73.54	2.031	0.4924	53.62	2.096	0.4771	39.17	2.198	0.4550
			3	73.54	.2031	4.924	53.62	.2096	4.771	39.17	.2198	4.550
			10	73.54	.06092	16.41	53.62	.06289	15.90	39.17	.06594	15.17
	100	20	1	58.81	0.1949	5.131	42.89	0.2012	4.970	31.34	0.2110	4.739
			5	58.81	.03898	25.65	42.89	.04024	24.85	31.34	.0422	23.70
			30	58.81	.006497	153.9	42.89	.006707	149.1	31.34	.007033	142.2
	300	20	1	176.4	0.5846	1.711	128.7	0.6037	1.656	94.00	0.6330	1.58
			5	176.4	.1169	8.554	128.7	.1267	8.285	94.00	.1266	7.899
		10	10	88.2	0.01462	68.40	64.4	0.01509	66.27	47.01	0.01583	63.17
		20	10	176.4	0.05846	17.11	128.7	0.06037	16.56	94.00	0.06330	15.80
			30	176.4	.01949	51.31	128.7	.02012	49.70	94.00	.02110	47.39
Drizzle	100	400	1	1176	77.96	0.01283	857.7	80.50	0.01242	626.7	84.42	0.01185
	300	400	10	3529	23.39	0.04275	2574	24.15	0.04141	1880	25.32	0.03949
			30	3529	7.797	.1283	2574	8.050	.1242	1880	8.440	.1185
Rain	300	1000	5	8823	292.4	0.003420	6434	301.8	0.003313	4701	316.6	0.003159
			10	8823	146.2	.006840	6434	150.9	.006627	4701	158.3	.006317
			30	8823	48.73	.020520	6434	50.30	.01988	4701	52.77	.01895

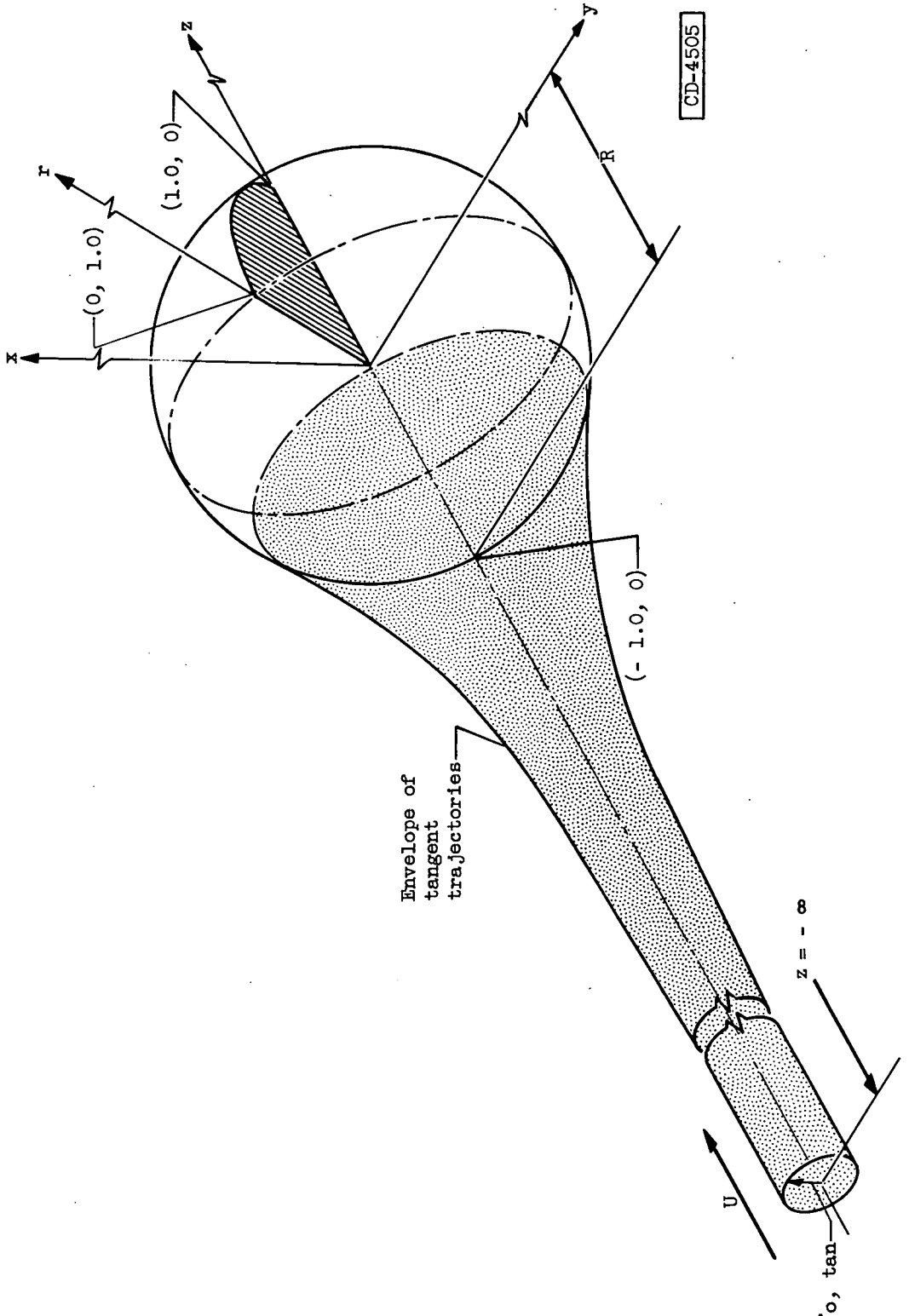

Figure 1. - Coordinate system for droplet-trajectory calculations about a sphere.

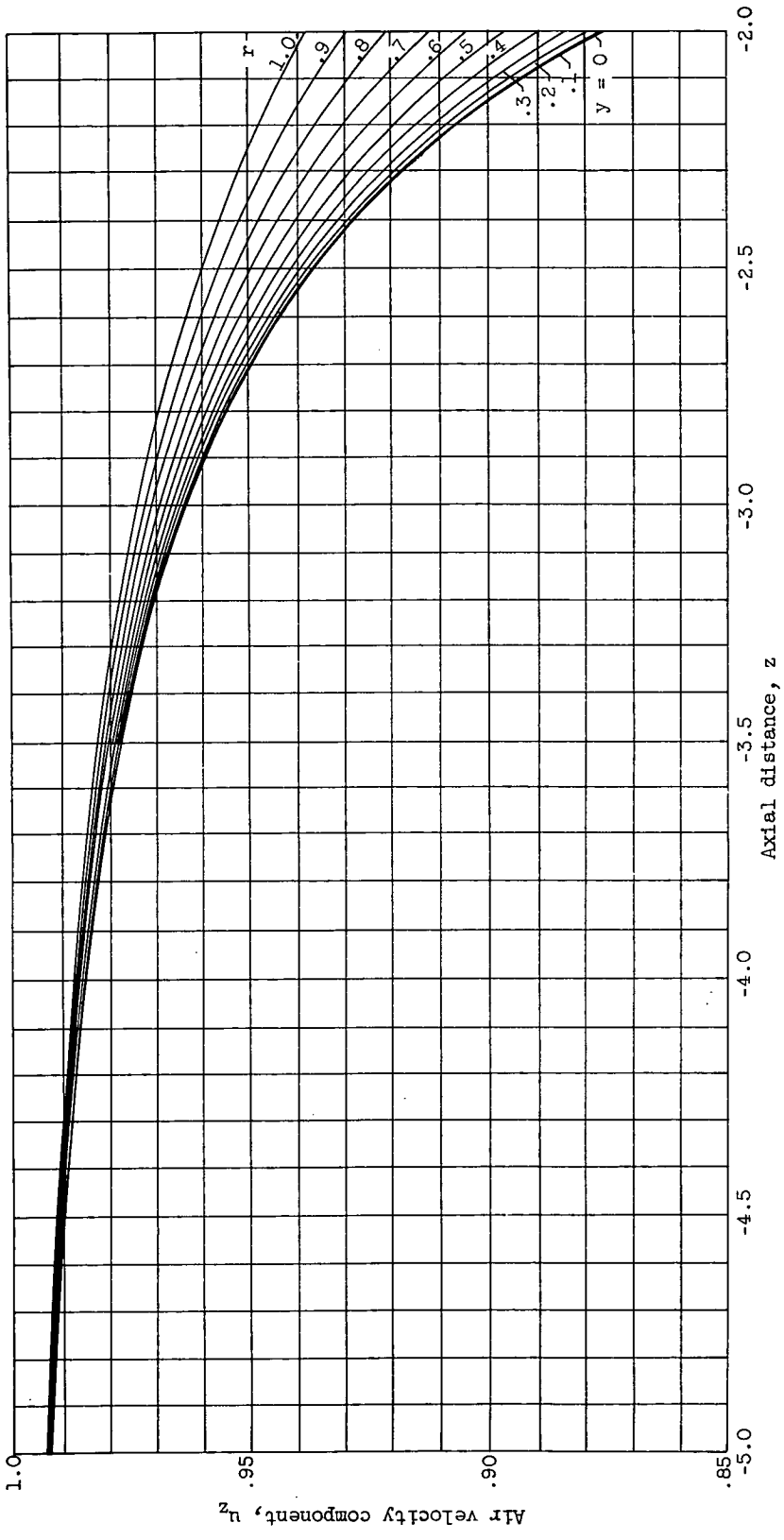

(a) z-Component of air velocity as function of z for constant values of r.

Figure 2. - Sphere flow field.

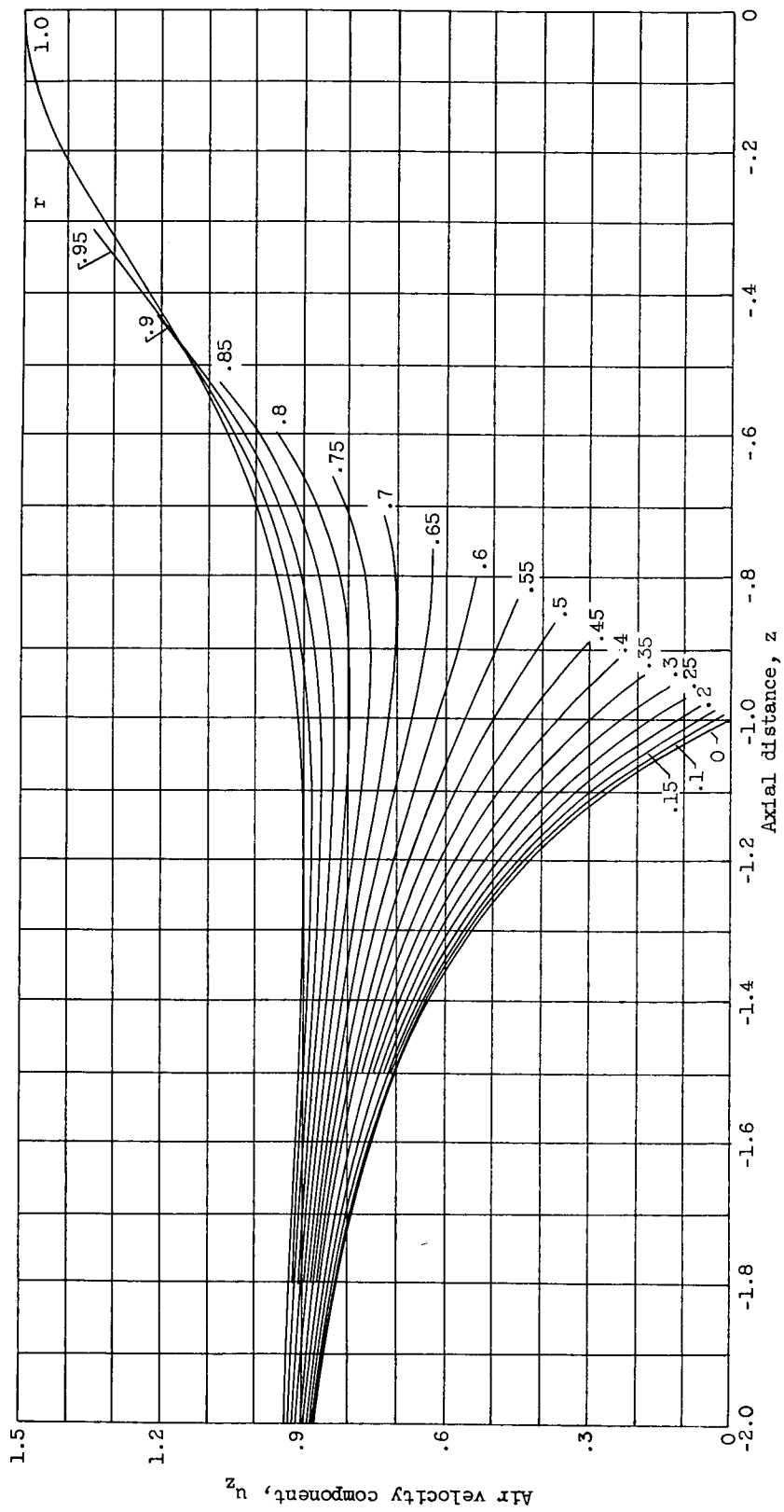

(a) Concluded. z-Component of air velocity as function of z for constant values of r.

Figure 2. - Continued. Sphere flow field.

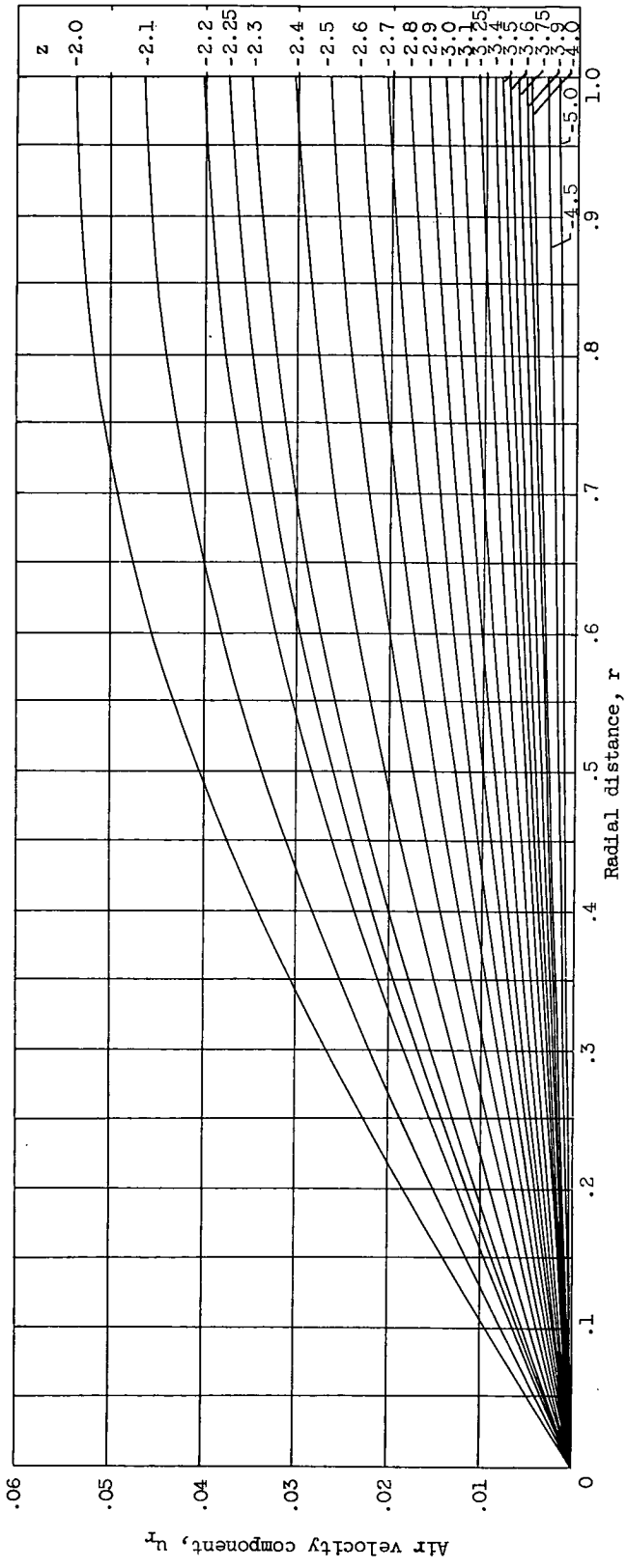

(b) r-Component of air velocity as a function of r for constant values of z.

Figure 2. - Continued. Sphere flow field.

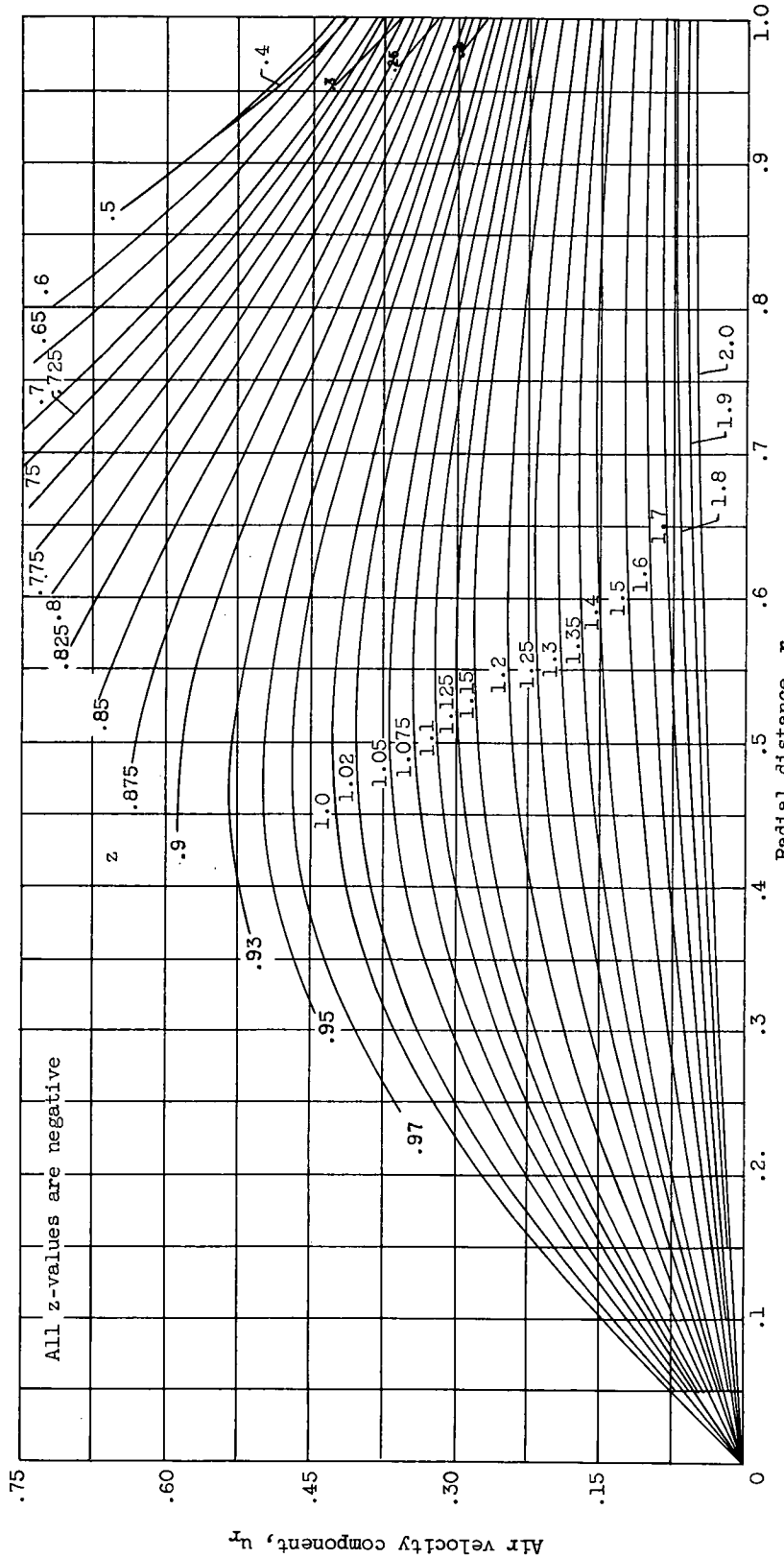

(b) Concluded. r-Component of air velocity as function of r for constant values of z.

Figure 2. - Concluded. Sphere flow field.

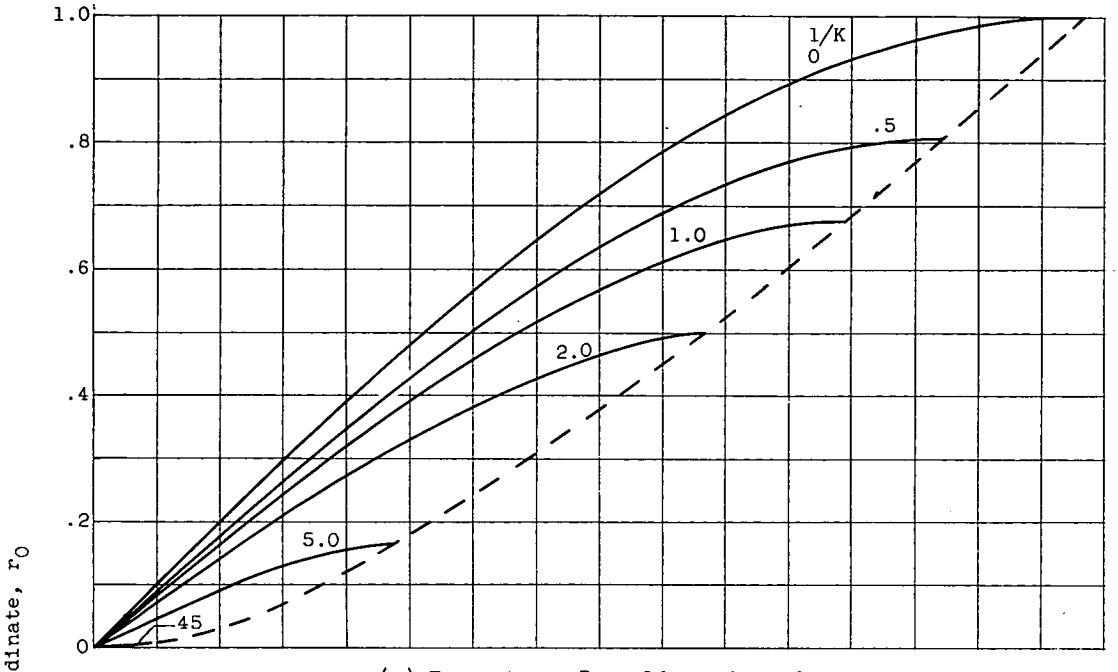

(a) Free-stream Reynolds number, 0.

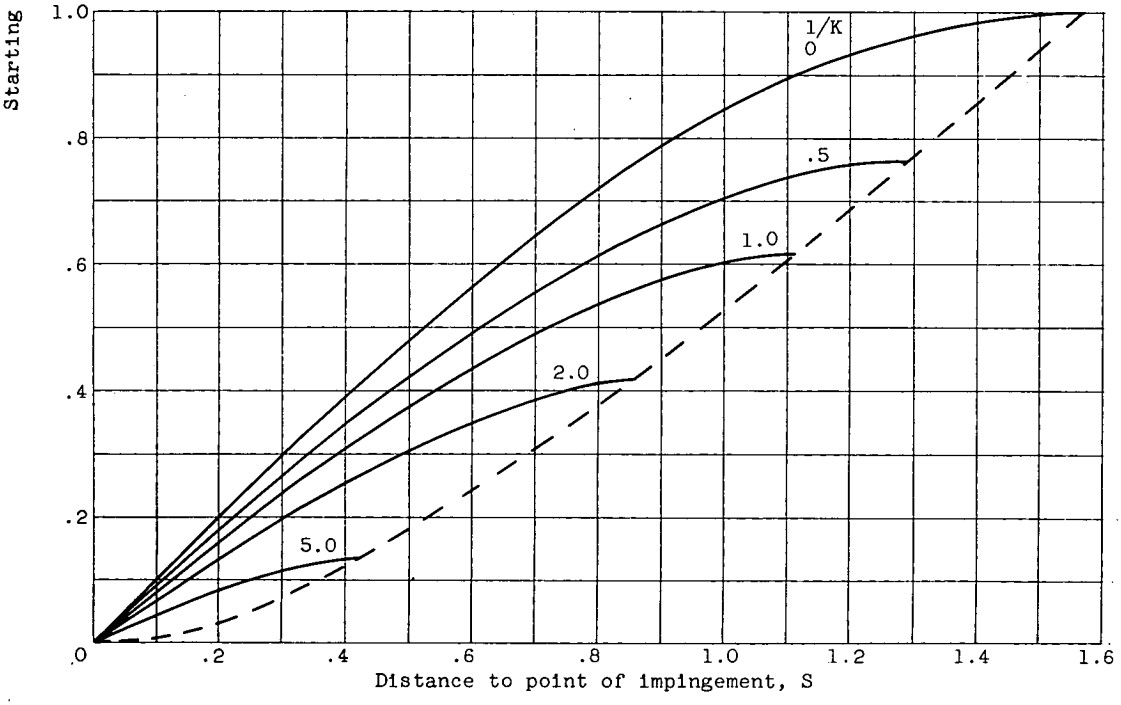

(b) Free-stream Reynolds number, 16.

Figure 3. - Starting ordinate as function of distance along surface to point of impingement.

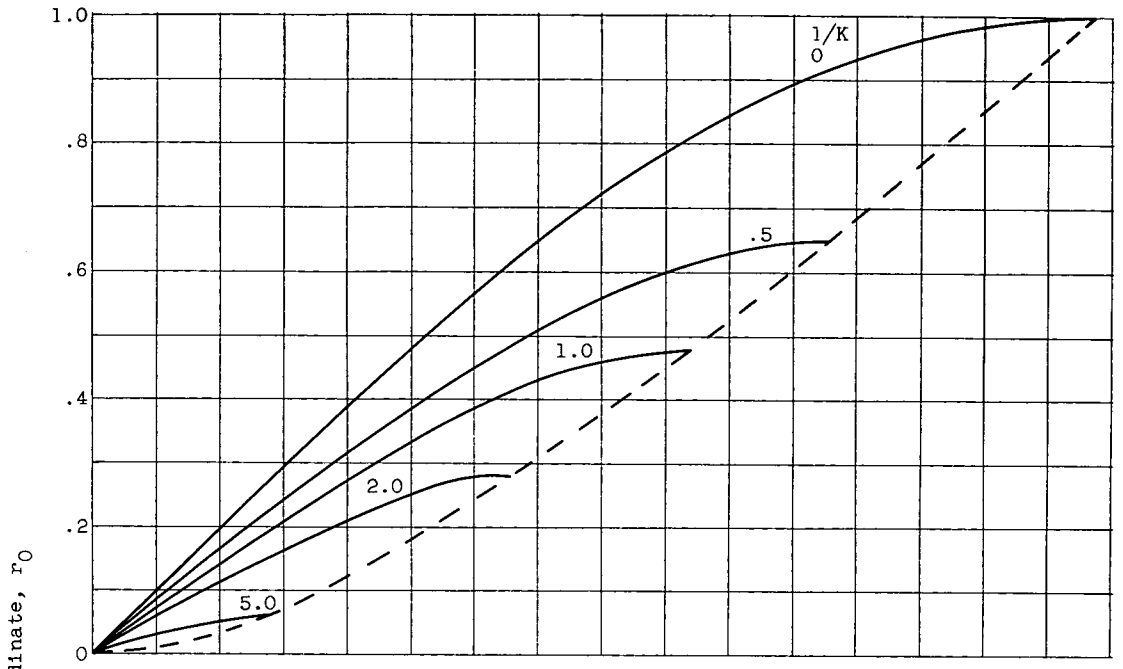

(c) Free-stream Reynolds number, 128.

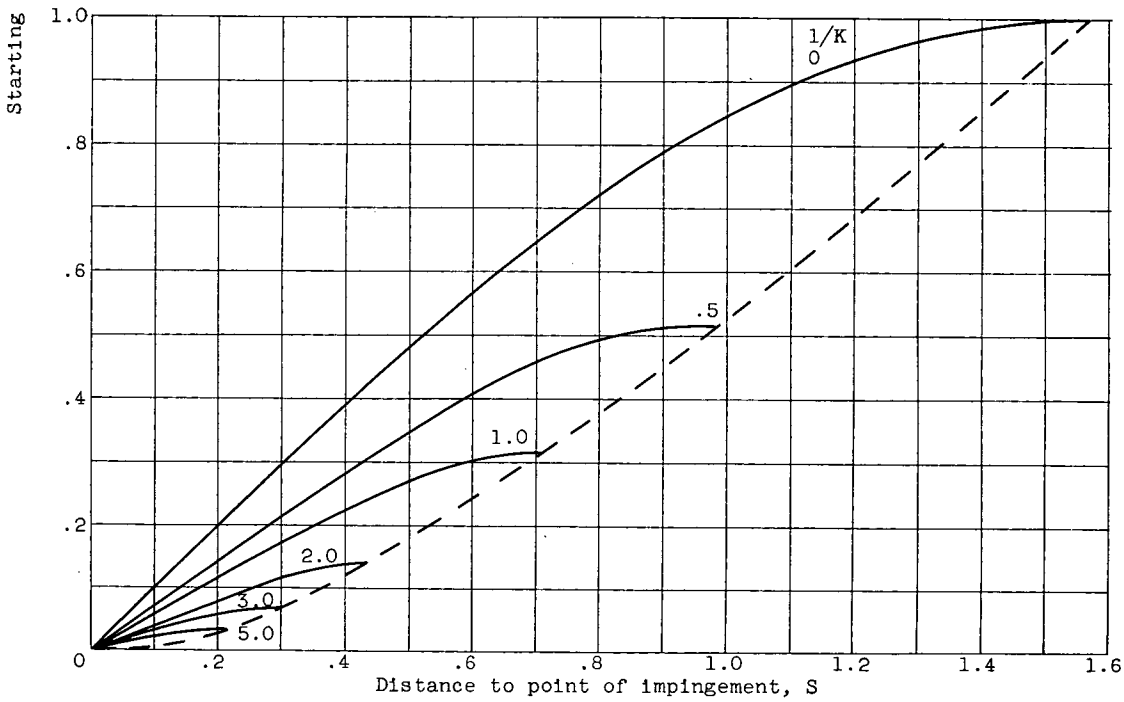

(d) Free-stream Reynolds number, 512.

Figure 3. - Continued. Starting ordinate as function of distance along surface to point of impingement.

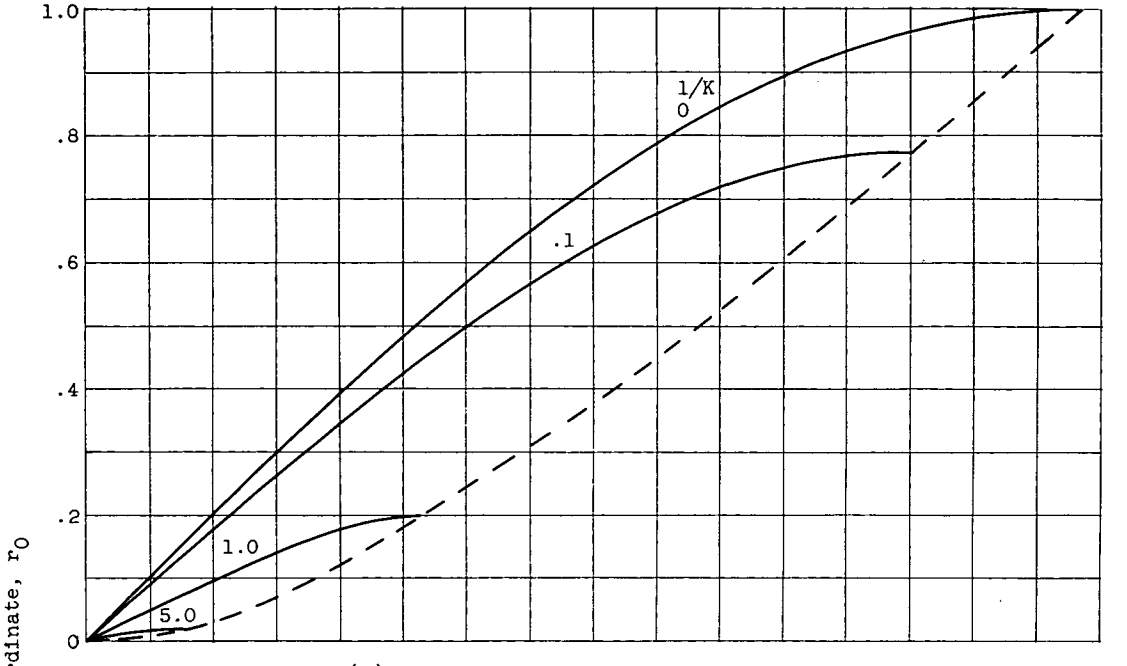

(e) Free-stream Reynolds number, 1024.

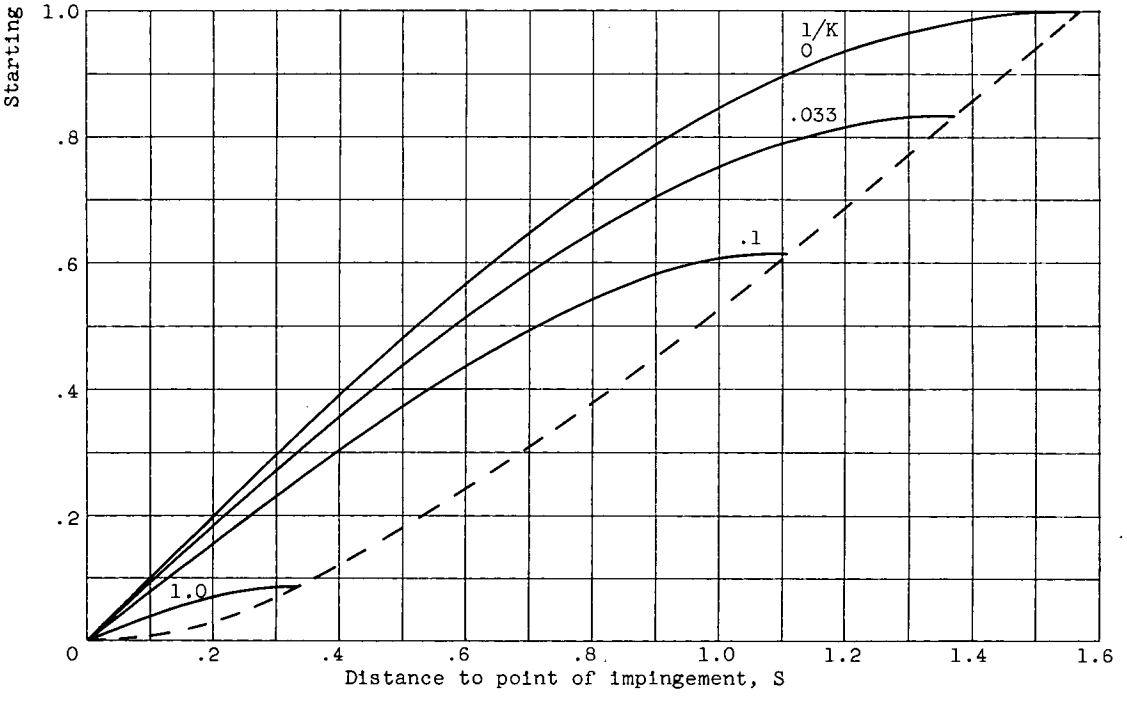

(f) Free-stream Reynolds number, 4096.

Figure 3. - Continued. Starting ordinate as function of distance along surface to point of impingement.

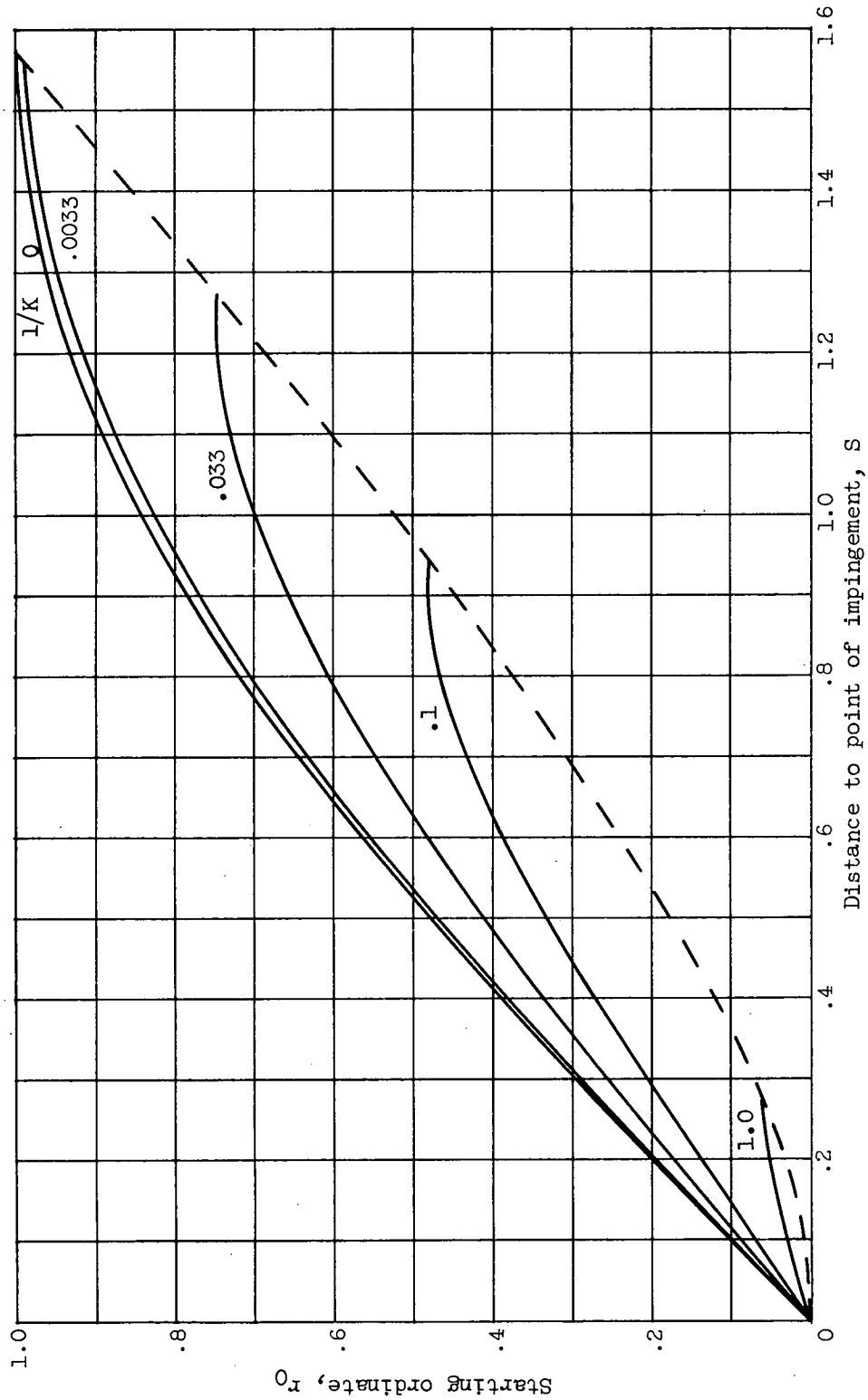

(g) Free-stream Reynolds number, 8192.

Figure 3. - Concluded. Starting ordinate as function of distance along surface to point of impingement.

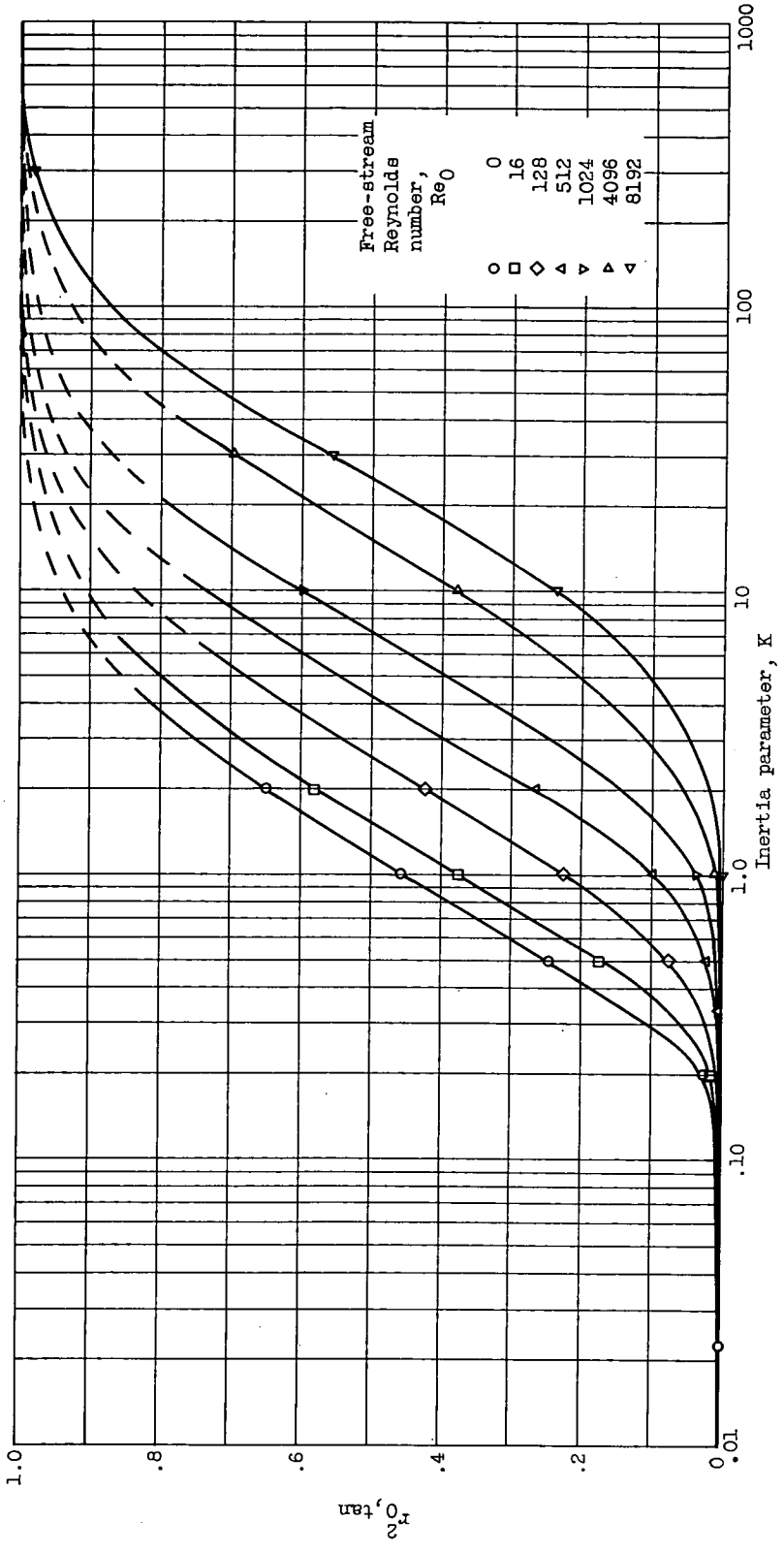

Figure 4. - Square of starting ordinate of tangent trajectory as function of inertia parameter.

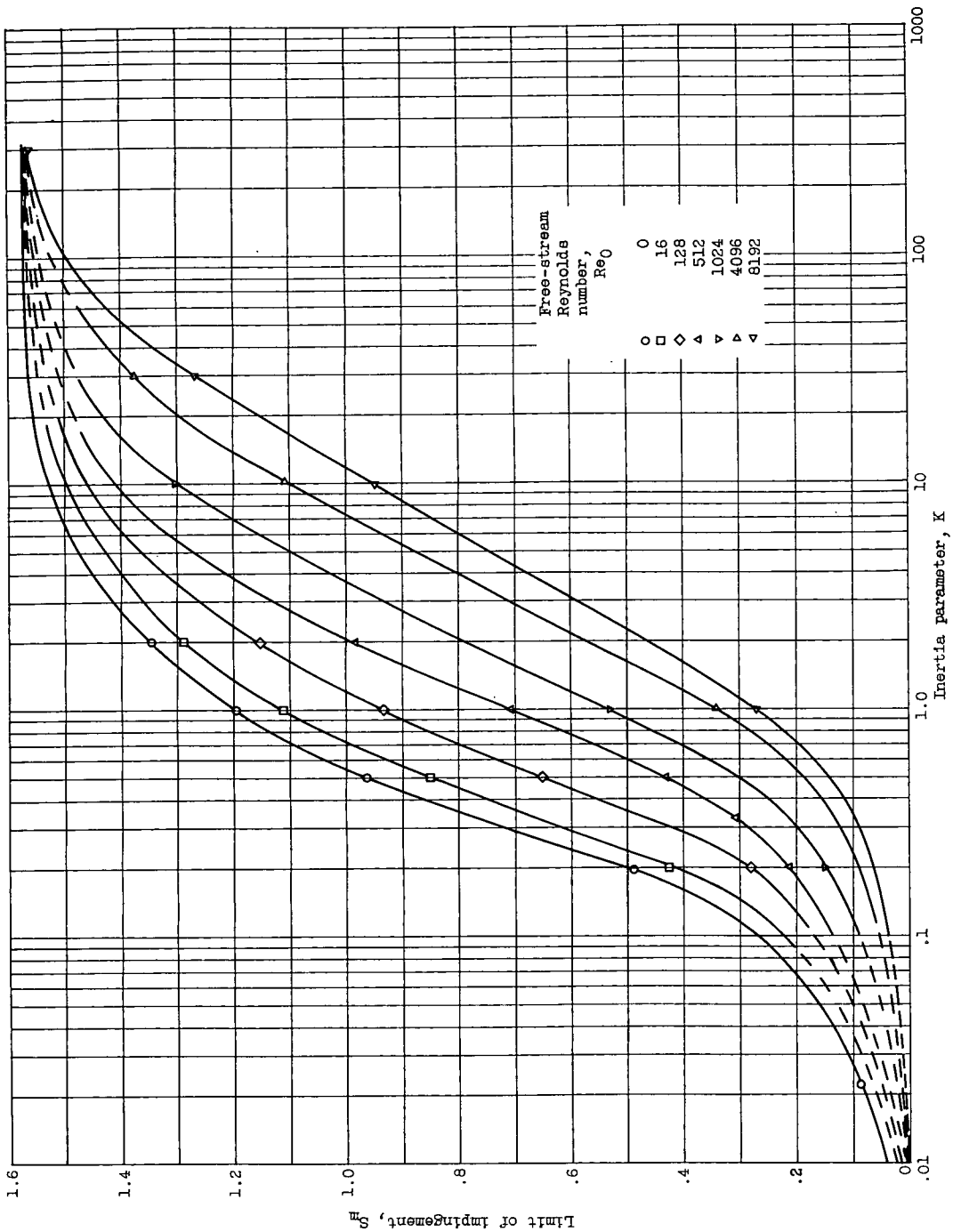

Figure 5. - Limit of impingement zone on surface of sphere.

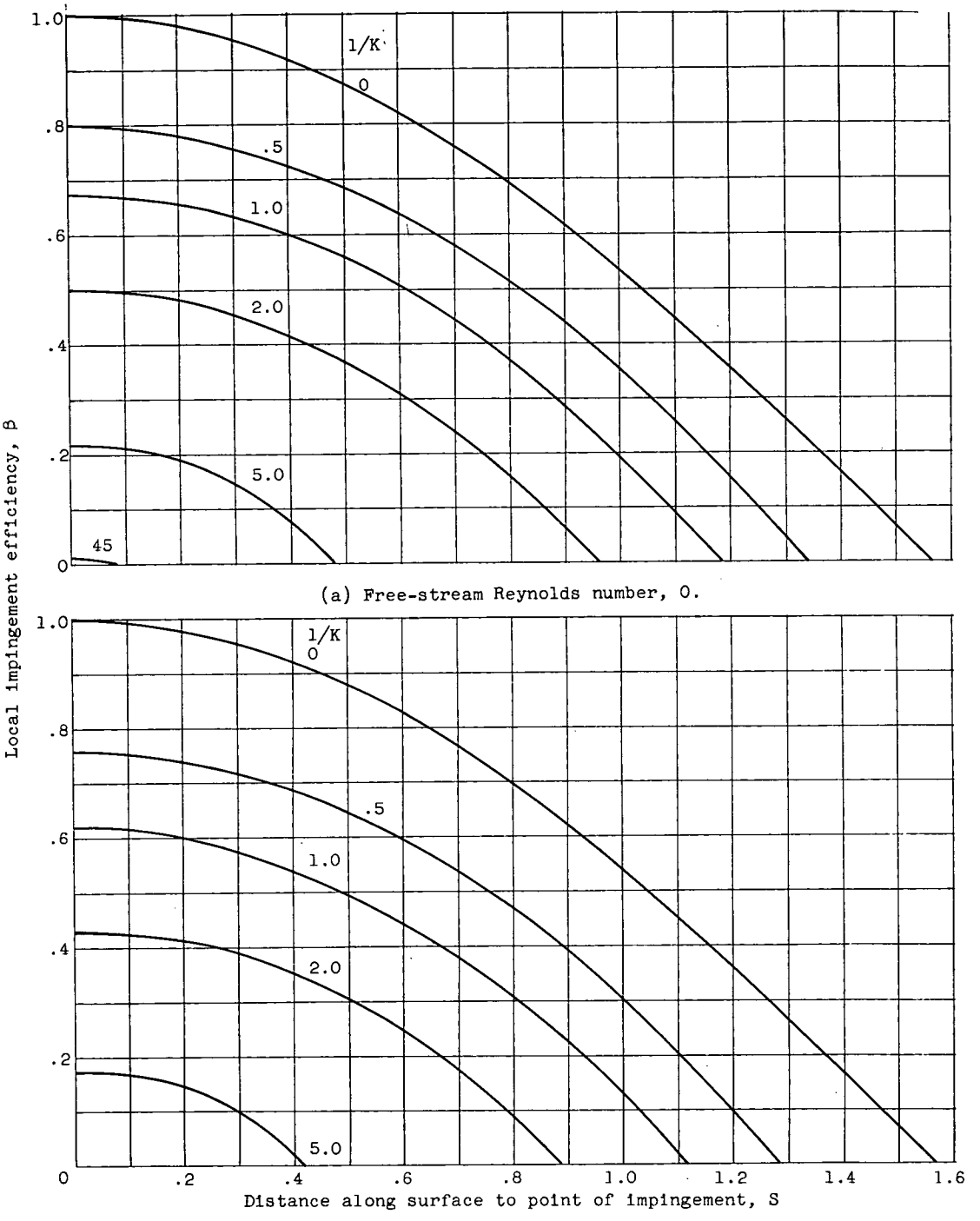

Figure 6. - Local impingement efficiency $\beta = \frac{r_0}{r}\frac{dr_0}{dS}$.

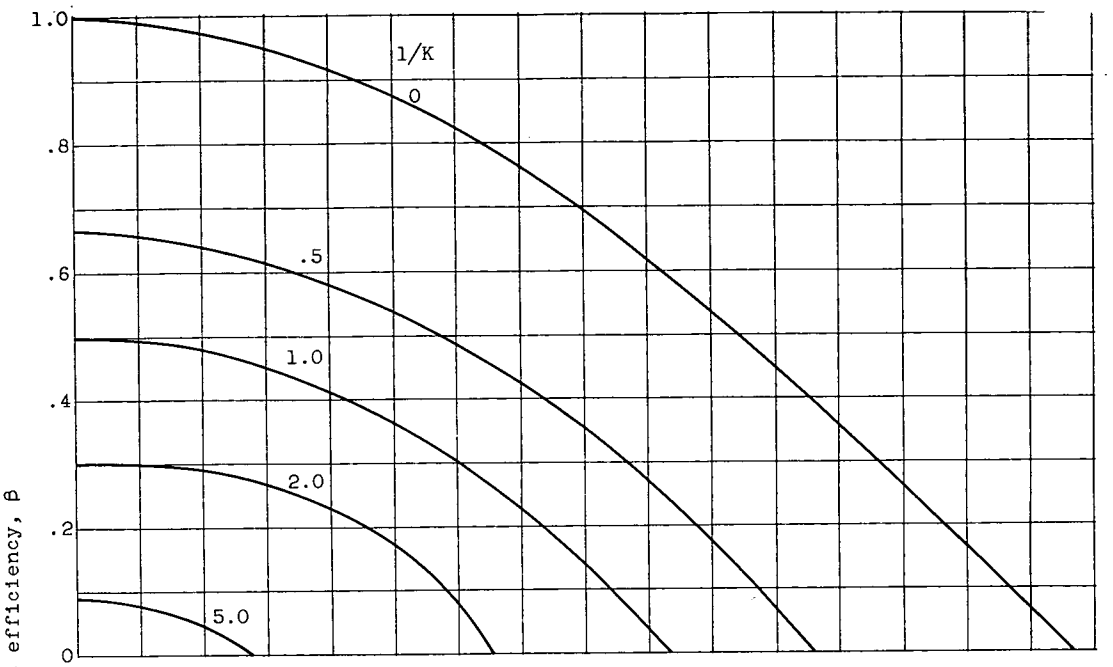

(c) Free-stream Reynolds number, 128.

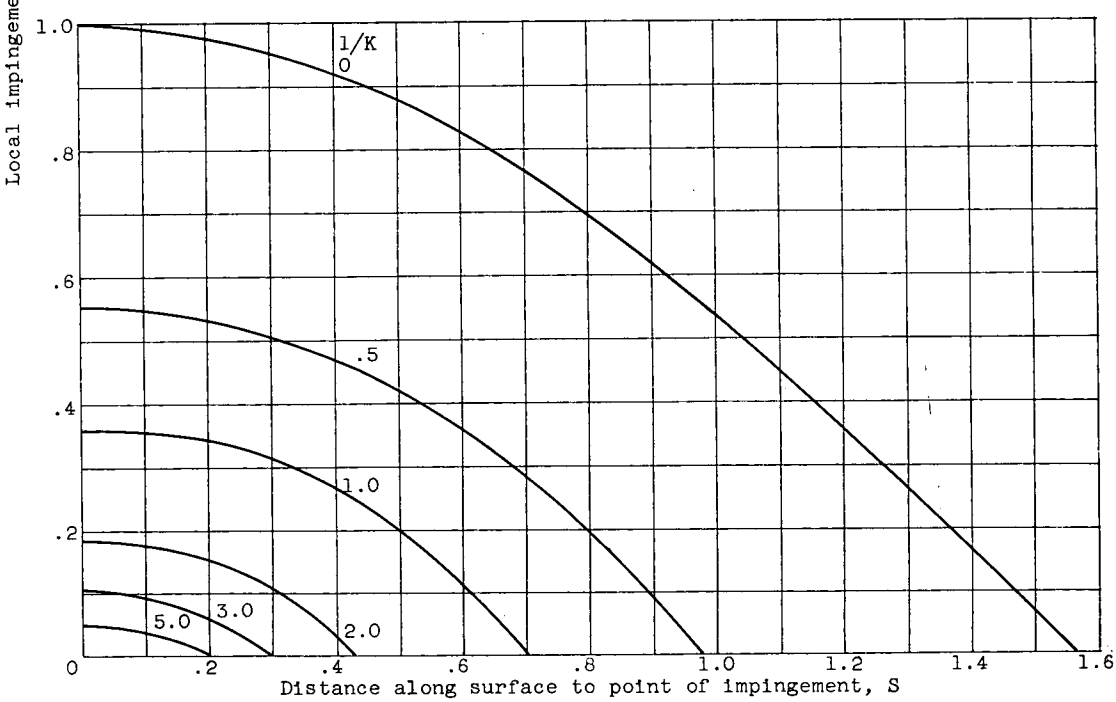

(d) Free-stream Reynolds number, 512.

Figure 6. - Continued. Local impingement efficiency $\beta = \frac{r_0}{r}\frac{dr_0}{dS}$.

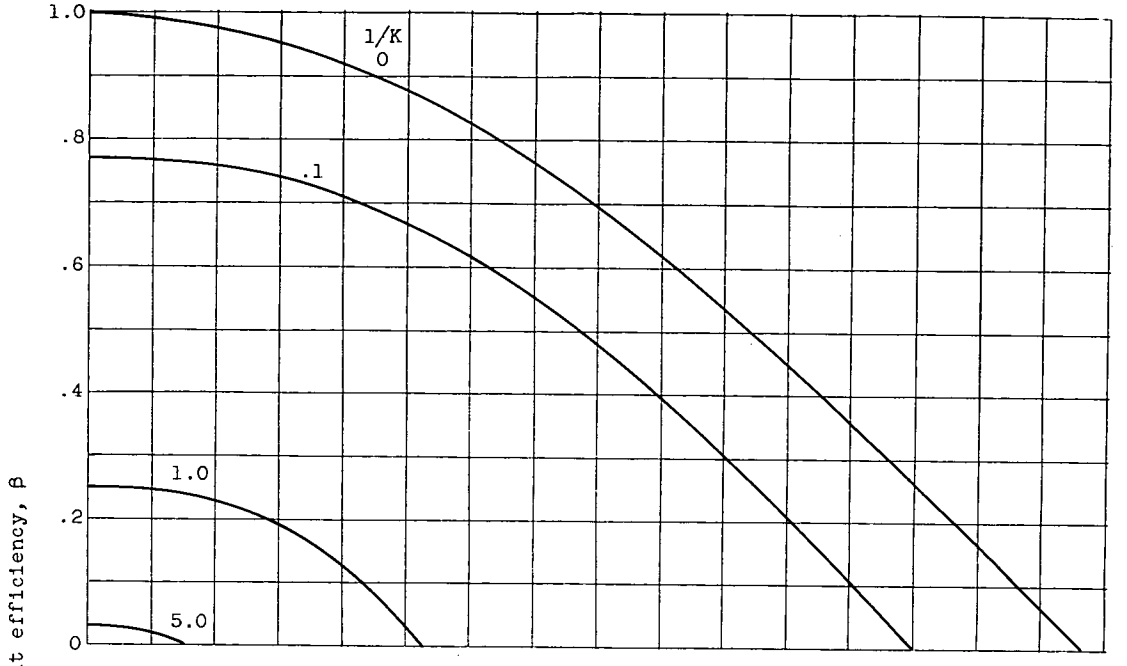

(e) Free-stream Reynolds number, 1024.

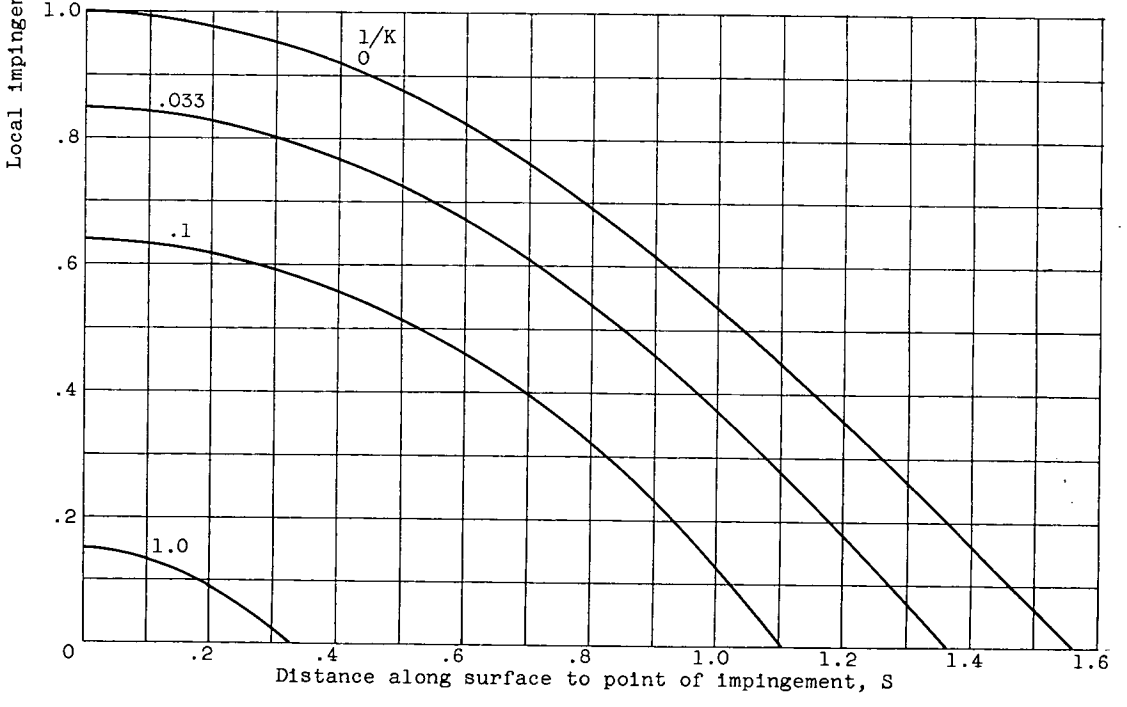

(f) Free-stream Reynolds number, 4096.

Figure 6. - Continued. Local impingement efficiency $\beta = \frac{r_0}{r}\frac{dr_0}{dS}$.

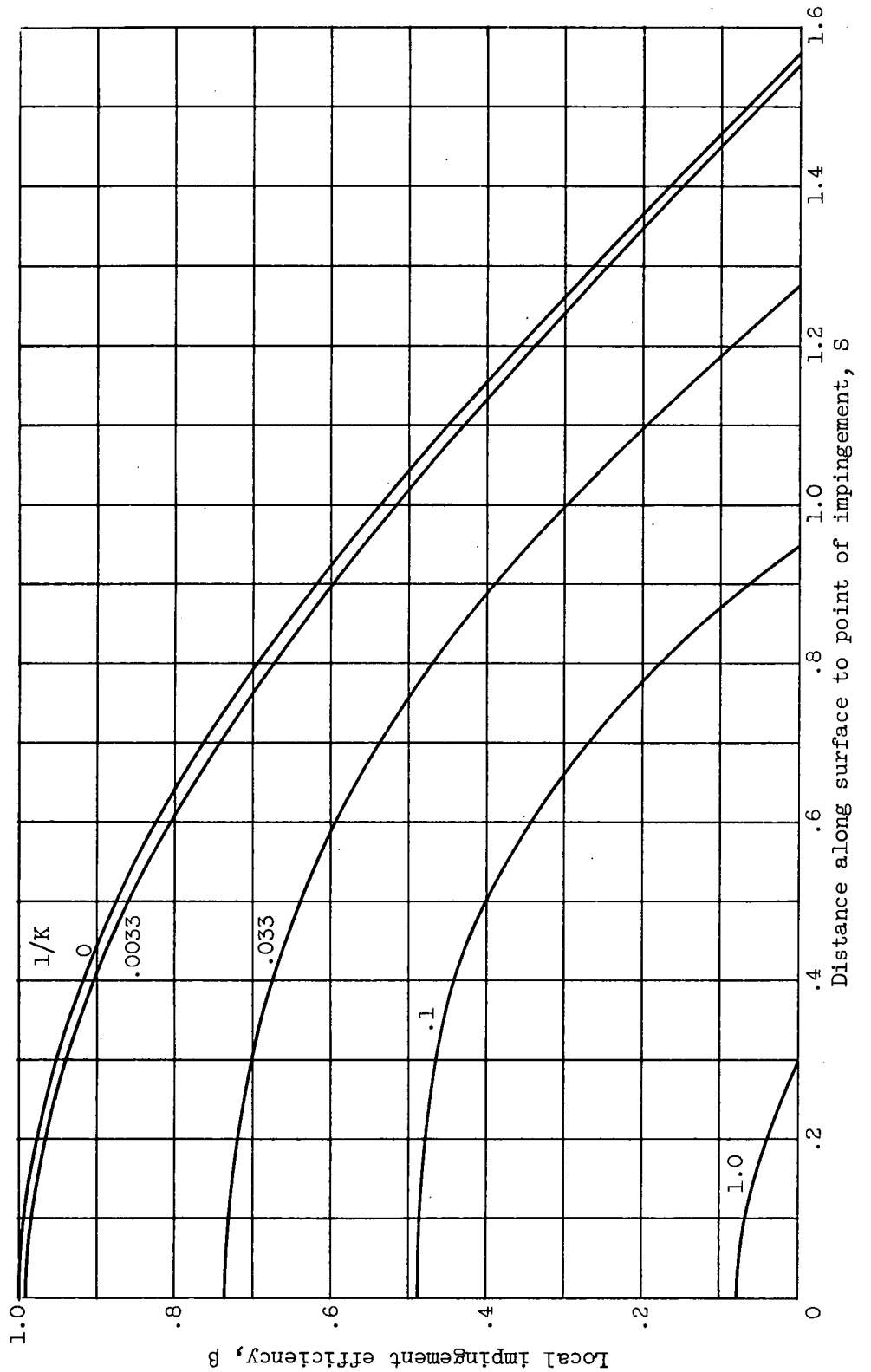

(g) Free-stream Reynolds number, 8192.

Figure 6. - Concluded. Local impingement efficiency $\beta = \frac{r_0}{r}\frac{dr_0}{dS}$.

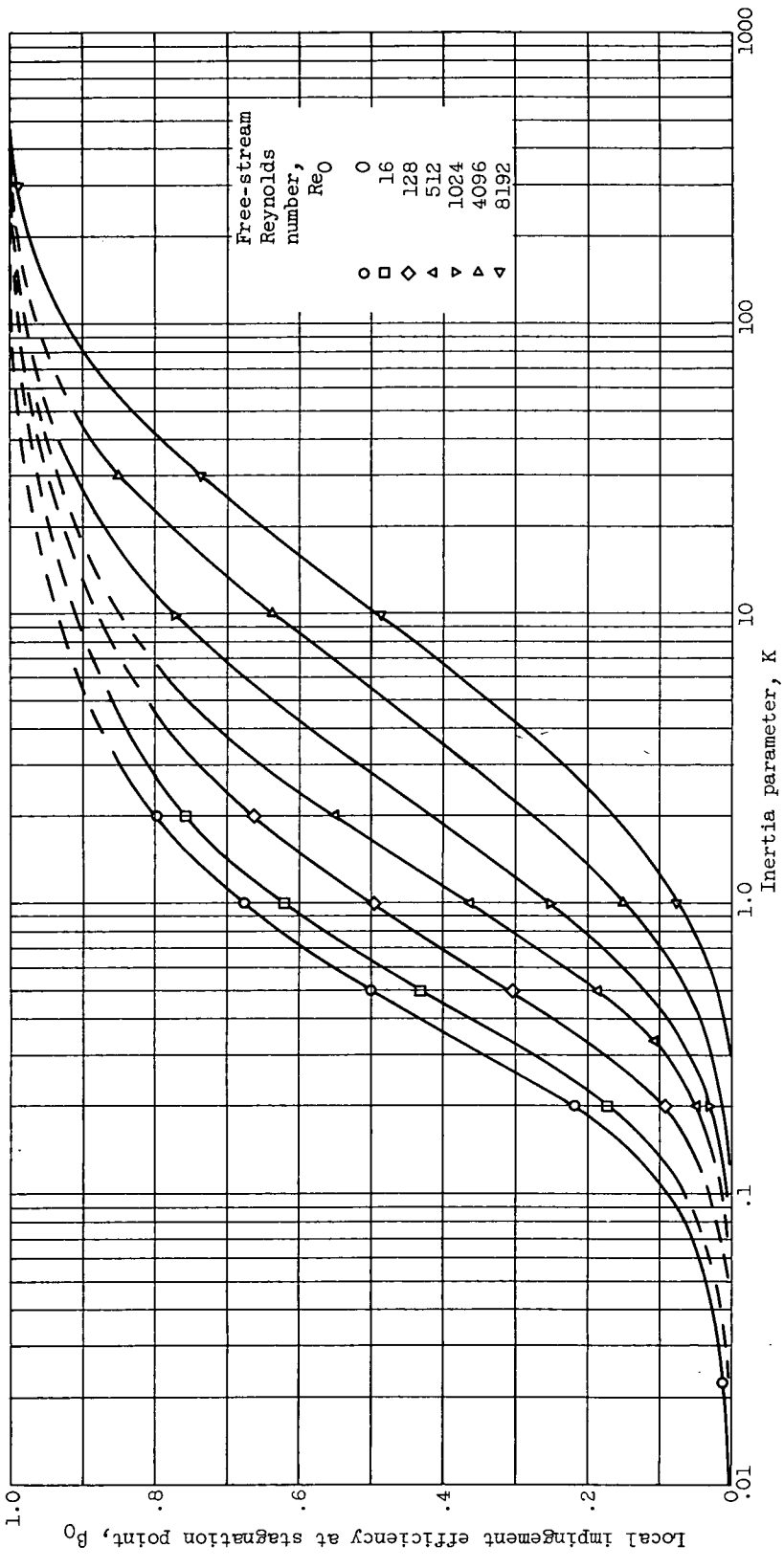

Figure 7. - Local impingement efficiency at stagnation point as function of inertia parameter.